# Correlation Effects in the Triangular Lattice Single-band System Li$_x$NbO$_2$

K.-W. Lee[1], J. Kuneš[2,3], R. T. Scalettar[1], and W. E. Pickett[1]

[1]*Department of Physics, University of California, Davis, California 95616, USA*

[2]*Theoretical Physics III, Center for Electronic Correlations and Magnetism,*
*Institute of Physics, University of Augsburg, Augsburg 86135, Germany and*

[3]*Institute of Physics, Academy of Sciences, Cukrovarnická 10, CZ-162 53 Prague 6, Czech Republic*

(Dated: July 26, 2007)

Superconductivity in hole-doped Li$_x$NbO$_2$ has been reported with $T_c \approx$5 K in the range 0.45 $\leq x <$ 0.8. The electronic structure is based on a two-dimensional triangular Nb lattice. The strong trigonal crystal field results in a single Nb $d_{z^2}$ band isolated within a wide gap, leading to a single-band triangular lattice system. The isolated, partially filled band has a width $W$=1.5 eV with dominant *second* neighbor hopping. To identify possible correlation effects, we apply DMFT(QMC) using on-site Coulomb repulsion $U$=0–3 eV, and check selected results using determinant QMC. For $U$ as small as 1 eV, the single particle spectrum displays a robust lower Hubbard band, suggesting the importance of correlation effects in Li$_x$NbO$_2$ even for $U \leq W$. At half-filling ($x$=0), a Mott transition occurs at $U_c \approx$1.5 eV. Coupling between the O $A_g$ phonon displacement and correlation effects is assessed.

## I. INTRODUCTION

Not long after the discovery of high temperature superconductivity in layered cuprate compounds, Geselbracht, Richardson, and Stacy discovered superconductivity at $x$=0.45 and 0.50 in the layered niobate Li$_x$NbO$_2$ with $T_c \approx$5 K.[1] Samples were obtained by removing Li (hence electrons) from band insulating LiNbO$_2$. This superconductivity has been confirmed in the range 0.45$\leq x \leq$0.79 with $T_c$ showing no significant dependence on Li concentration,[1–4] but no superconductivity in the weakly doped range between $x$=0.84 and $x$=1.[3] Hall effect measurements confirmed hole-type carriers,[5] consistent with LiNbO$_2$ being a band insulator. The difficulty in synthesizing materials with $x <$0.45 may be related to the considerable covalency of Li along $c$-direction that is reflected in the Born effective charge.[6, 7]

Recently, Liu *et al.* revisited the superconductor ($x$=0.68) using specific heat measurements.[4] The electronic specific heat can be fit well using the BCS-type $s$-wave symmetry pairing. Additionally, the linear specific heat coefficient $\gamma_{exp}$=3.59 mJ/mol K$^2$ and the Debye temperature 462 K were obtained. The virtual crystal approximation (Li nuclear charge $Z = 2 + x$), leads to the band structure value $\gamma_b$=2.425 mJ/mol K$^2$ at $x = 0.68$, corresponding to weak electron-phonon coupling strength $\lambda = \frac{\gamma_{exp}}{\gamma_b} - 1 \approx$0.48, which could however be enough to account for $T_c \approx$ 5 K. The electron-phonon mechanism is consistent with stated theoretical viewpoints.[6, 8]

There are two interesting sister materials. An isostructural and isovalent Na$_x$NbO$_2$ has been observed to be superconducting with a little lower $T_c \approx$4 K, in the range $0.5 \leq x \leq 0.7$.[9, 10] Interpreted as an isotope shift, $\alpha = -d(lnT_c)/d(lnM)$ (M=mass) is 0.27. This value might be thought to imply phonon-mediated pairing, but the important coupling is not expected to be to the Li (Na) ion. Another system is H$_x$LiNbO$_2$, showing superconductivity with $T_c$=5 K at $x$=0.3 and 0.5.[11] Due to lack of structure studies as well as doping studies, the mechanism and what role H plays are not yet resolved.

In the $\mathcal{M}$(S,Se)$_2$ system with a transition metal $\mathcal{M}$, competition between a charge density wave transition (CDW) and superconductivity is frequently observed. Recently, Morosan *et al.* synthesized Cu$_x$TiSe$_2$.[12] By intercalating Cu (i.e., electron donation from Cu), the CDW is suppressed and this system becomes superconducting with the maximum $T_c \approx$4 K at $x = 0.08$. The Wilson ratio $R \sim 0.35$ is small, implying the importance of correlation effects. Another compound for comparison is Na$_x$CoO$_2$, which becomes a superconductor at $x \sim 1/3$ by intercalating water. Also, the dehydrated compound displays an interesting phase diagram with unique insulating phase at $x = 0.5$ and shows large correlation effects. As intensively studied by some of the present authors,[13] correlation effects in this system lead to charge disproportionation on the Co sublattice.

In addition to the common layered structure, both $\mathcal{M}$(S,Se)$_2$ and Cu$_x$TiSe$_2$ have an edge-sharing octahedral framework, similar with NbO$_6$ trigonal prismatic coordination in Li$_x$NbO$_2$. These similarities imply the significance of correlation effects in this niobate. At $x = 0$ (NbO$_2$) Nb has only one valence electron ($4d^1$) and the possibility of a Mott transition naturally arises. The observed structure of

NbO$_2$ is distorted rutile,[14] and the layered form may not be accessible experimentally.

In this paper, we investigate correlation effects on the presumed Mott insulating and nonstoichiometric phases using the dynamical mean field theory approximation (DMFT).[15] Selected results are compared with determinant quantum Monte Carlo calculations, where intersite correlations are included and the only limitations are the lattice size and the temperature. For varying strength of repulsion (whose value is not known), and for fillings $n$=1, 4/3, and 5/3 (note $n = x + 1$) we obtain the spectral density, and at $n$=1 we identify the critical strength for a metal- insulator transition, and display the evolution of system characteristics through the transition. Finally, we present changes in the spectral density due to (frozen) $A_g$ phonon displacements.

The triangular lattice aspect itself has assumed renewed interest, due in part to the discovery of superconductivity in the Na$_x$CoO$_2$ system. The nearest-neighbor triangular Hubbard model has been studied to uncover how it differs from the square lattice that is used as a model of the high temperature superconductors; its non-bipartite nature is found to be important in frustrating local spin correlations. We will compare results for Li$_x$NbO$_2$ where 2nd neighbor coupling dominates, to the same dynamical mean field approximation calculations for the nearest-neighbor case of Aryanpour and collaborators.[16]

## II. STRUCTURE AND CALCULATION

LiNbO$_2$ is based on a double-layered hexagonal structure ($P6_3/mmc$, No. 194) with lattice parameters $a$=2.90 Å and $c$=10.46 Å.[2, 3, 17–20] Li and Nb atoms lie on $2a$ sites $(0,0,0)$ and $2d$ sites $(\frac{2}{3},\frac{1}{3},\frac{1}{4})$, respectively. O atoms occupy $4f$ sites $(\frac{1}{3},\frac{2}{3},z)$. In this material, NbO$_6$ units place the Nb ion in trigonal prismatic coordination. The O internal parameter $z$, which is measured from the Li layers, shows some disagreement between reports, and our calculations use the experimental value $z$=0.1263[18] for which the electronic structure was analyzed earlier.[6] This value leads to Nb-O bond length 2.116 Å, and O-Nb-O bond angles 86.5° and 75.4°.

We have carried out first principles, local density approximation (LDA) calculations using the full-potential local-orbital code (FPLO),[21] and the results are consistent with previous reports.[6, 7] The basis set was Li $(1s)2s2p3d$, Nb $(4s4p)5s5p4d$, and O $2s2p3d$. (The orbitals in parentheses indicate semicore orbitals.) As reported previously,[6, 8] the electronic structure shows strong two-dimensionality and for our investigation of correlation effects we
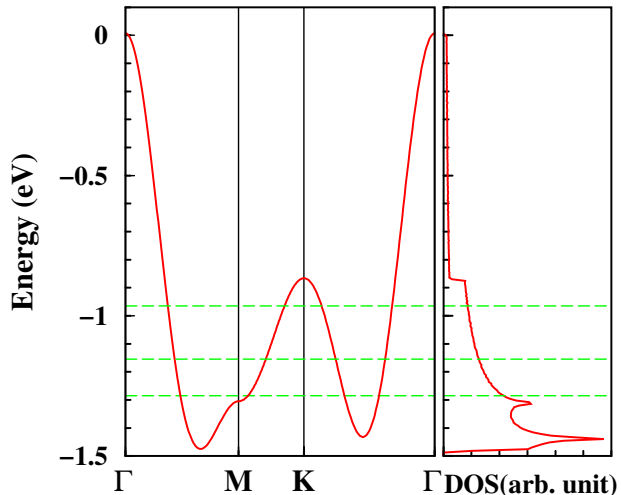


FIG. 1: (Color online) Two-dimensional tight-binding band structure and density of states, using up to third neighbor hopping parameters ($t_1$=64, $t_2$=100, and $t_3$=33 meV), for the single isolated $d_{z^2}$ state in LiNbO$_2$. The dashed horizontal lines indicate the Fermi energy $E_F$ in the rigid band picture for electron fillings $n$=1, 4/3, and 5/3 from bottom to top. The centroid of the band $E_0$ lies on 18 meV below $E_F$ for $n$=4/3. Note lower half of weight is localized within 0.2 eV width, only 13 % of the total bandwidth.

neglect the $k_z$ dispersion. Our DMFT calculations were carried with two-dimensional tight-binding (TB) parameters $t_1$=64, $t_2$=100, and $t_3$=33 meV, leading to bandwidth $W$=1.5 eV. These hopping parameters were obtained using Wannier function techniques.[6] The TB band structure and DOS are displayed in Fig. 1.

Studies of lithium-deintercalation in the range $0.5 \leq x \leq 1$ by Kumada et al. display negligible change in the structure parameters including Nb-O bond length.[17] This behavior is consistent with the observation that the electronic structure follows a rigid band model well.[6, 8, 20] Thus these tight-binding parameters will be used for all $x$. (Since another structure[14] is observed, $2H$–NbO$_2$ as considered here would be at best a metastable state.)

Hirsch-Fye quantum Monte Carlo (QMC) DMFT calculations[15] were carried out to investigate dynamic correlation effects, applying the on-site Coulomb repulsion $U$ less than 3 eV to the single isolated $d_{z^2}$ Wannier function. The DMFT study is based on the Hubbard model

$$H = \sum_{i,j,\sigma} t_{ij}(c_{i\sigma}^+ c_{j\sigma} + c_{j\sigma}^+ c_{i\sigma}) - \mu \sum_{i\sigma} n_{i\sigma}$$
$$+ U \sum_i n_{i\uparrow} n_{i\downarrow} \qquad (1)$$

with the hopping parameters $t_{ij}$ between site $i$ and $j$,

the chemical potential $\mu$, the spin quantum number $\sigma$, $c_{j\sigma}^{+}$ creates an electron of spin $\sigma$ at site $j$, and $n_{i\sigma} \equiv c_{i\sigma}^{+}c_{i\sigma}$ is the number operator. The results reported here are for $T$=1100 K (i.e., 0.1 eV). 40–100 time-slices are used for the QMC runs.

The spectral density $A(\omega)$ has been obtained using the maximum-entropy (MaxEnt) analytic continuation technique developed by Jarrell and Gubernatis.[22] In MaxEnt good QMC data, close to Gaussian distribution, are crucial. We checked the statistics up to $12 \times 10^6$ sweeps and also about 500 $k$-points in the two-dimensional irreducible wedge. However, at small and large $U$ regimes, the spectral densities, specially near $\omega = 0$, depend noticeably on the convergence parameters. In this paper we will show the results in range of $U$=0.5–2.5 eV, which shows robust results for $A(\omega)$. MaxEnt can be performed in a few different ways. In our calculations, both classic and Bryan techniques have been used and show consistent results. The other ingredient in MaxEnt is the default model for the spectral density.[22] Since the default model is immaterial for good data, two different ways based on a Gaussian model were tried. One is independently calculated using the same default model for each $U$, and the other way is that a converged result for previous higher $U$ value is used as a default model for next small $U$. These methods give consistent results, indicating the robustness of results from the MaxEnt technique.

The bulk of our results have been obtained with this DMFT approach. To assess whether intersite correlations may affect our conclusions, we complement them with a limited set of simulations using determinant quantum Monte Carlo (DQMC) [23], performed for the same Hamiltonian, Eq. 1 but on finite spatial lattices. This approach includes the momentum dependence of the self energy, but has the drawback of not working in the thermodynamic limit, as DMFT does. As in the DMFT QMC solver, DQMC requires a discretization of the inverse temperature $\beta$. We have chosen the interval $\Delta\tau = 0.5$ which satisfies the condition $t_i U(\Delta\tau)^2 << 1$ required for the 'Trotter errors' associated with the discretization to be small. Our runs typically used 2,000 sweeps to equilibrate the lattice and 20,000 sweeps to take measurements. We have looked at the density and short range spin correlations on $12 \times 12$ lattices in addition to the $9 \times 9$ lattice results shown here, and observe only minor changes.
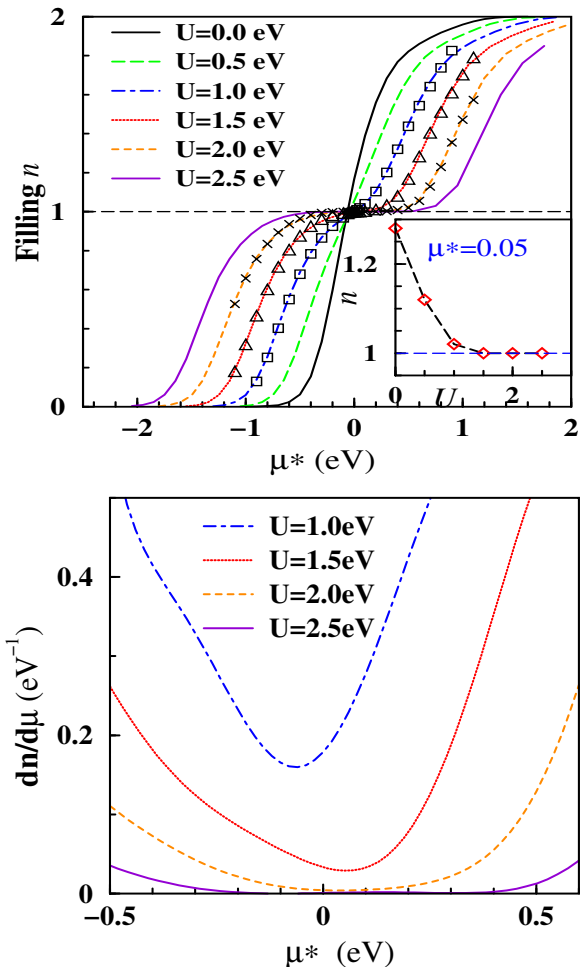
FIG. 2: (Color online) Top: Electron filling $n$ versus effective chemical potential $\mu^* = \mu - U/2$, when changing the on-site Coulomb repulsion $U$. The lines and symbols are the results of DMFT and DQMC calculations respectively. The excellent agreement is partly a consequence of the magnetic frustration of the triangular lattice which diminishes the importance of including intersite correlations (see text). Even for $U$=1.0 eV, the slope changes significantly near half-filling, which is indicated by the dashed horizontal line. Above $U$=1.5 eV, there is a plateau at half-filling. Inset: $n$ vs. $U$ plot at $\mu^*$=0.05, which displays clearly a metal-to-insulator transition completing ($n \to 1$) near $U$=1.5 eV. Bottom: Compressibility $\kappa \equiv dn/d\mu$ versus $\mu^*$ near the critical $U$ regime, showing more clearly where it approaches and becomes vanishingly small.

## III. METAL-INSULATOR TRANSITION

### A. Electron Filling versus Chemical Potential

We first address the metal-insulator transition (MIT) at half-filling. When a gap exists, the occu-
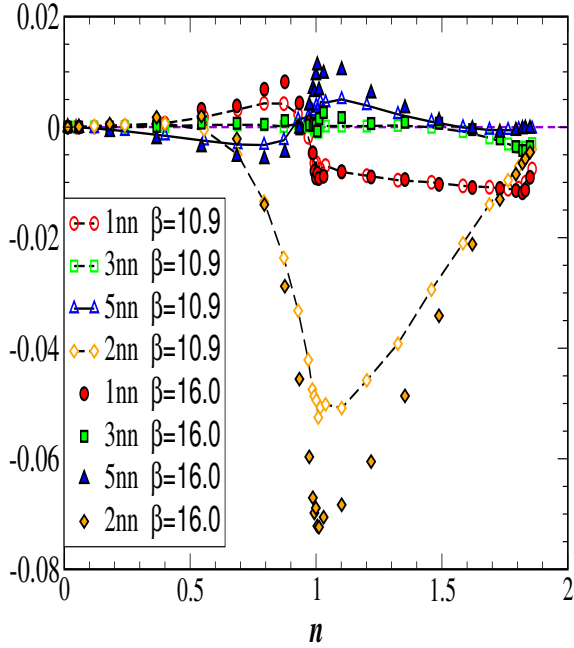
FIG. 3: (Color online) Determinant QMC result for the spin-spin correlation function for temperatures of 1100 K ($\beta$=10.9) and 750 K ($\beta$=16), versus versus band filling $n$. $U$=1, and energies are in eV. The 5th neighbor (5nn) is the third neighbor along a straight line from the reference site.

pied electron density remains unchanged for values of the chemical potential $\mu$ within the gap. This behavior can be observed as a plateau in electron filling $n(\mu)$ plots as $U$ is increased, and is displayed in the top panel of Fig. 2. Since there is a Hartree-Fock-like shift of the entire spectrum with $U$ for the form of Hamiltonian we use, the chemical potential is shifted simply by $U/2$ and denoted by $\mu^*$. Already at $U$=1 eV, an inflection is clear near half-filling. This inflection point becomes a plateau of $\sim$0.1 eV width at $U$=1.5 eV, indicating proximity to the MIT.

The critical coupling strength $U_c$ for the MIT can be determined more precisely using two different methods. First, choosing $\mu^*$=0.05 eV (chosen somewhat above $\mu^* = 0$ for clarity), the filling approaches unity as $U \rightarrow$1.5 eV, as shown in inset of Fig. 2 (top panel). Second, and most clearly, vanishing compressibility $\kappa = dn/d\mu$ signifies the onset of the insulating phase. The bottom panel of Fig. 2 shows $\kappa$ is reduced by an order of magnitude for $U$=1.5 eV, but only truly vanishes for $U$ close to 2 eV. It must be recalled however that the calculations are done at T=0.1 eV, and temperature broadening is $\sim \pi$T in addition to other temperature effects, so requiring $\kappa$ to vanish overestimates $U_c$. Considering the $n(\mu^*)$ plot in the inset of Fig. 2, we identify $U_c \approx 1.5$ eV as the (low temperature) critical strength.

Figure 3 shows the intersite spin correlations $< S_i^+ S_j^- >$, obtained with DQMC on a 9×9 lattice. Two temperatures are shown, $T = 1100$K and $T = 750$ K. The dominant tendency is toward antiferromagnetic orientation between 2nd neighbor spins connected by $t_2$, which is certainly reasonable given that it is the largest hopping, and hence has the largest value of $J = 4t^2/U$. This short-range order increases strongly as $T$ is lowered, and the asymmetry around half-filling becomes sharp and more pronounced. Near neighbor spins, connected by $t_1$, have a correlation which is almost an order of magnitude smaller, and its increase with lowering temperature is less pronounced. This small near neighbor correlation is strongly dependent on band filling, being ferromagnetic for $n < 1$ and antiferromagnetic for $n > 1$. Interestingly, while the 3rd neighbor spins connected by $t_3$ are essentially uncorrelated, spins which are separated linearly by three lattice constants (5th neighbors), for which there is no direct hopping, exhibit significant antiferromagnetic correlations for $n < 1$ and ferromagnetic correlations for $n > 1$, *i.e. opposite* in sign to the near neighbor correlation. Overall, the local spin order is markedly different on the two sides of half-filling, $n = 1$, in contrast to the square lattice (and bipartite lattices generally) where the order is symmetric about half-filling.

Coupling to second neighbors alone (as occurs here, crudely speaking) separates the triangular lattice into three independent triangular sublattices, each with lattice constant $\sqrt{3}a$. On each sublattice there are "near neighbor" antiferromagnetic correlations, which are frustrated on the triangular lattice. Near neighbor hopping couples a given site to three sites of each of the other sublattices, and antiferromagnetic 1nn coupling tends to add to the frustration. Third neighbor hopping also connects to three sites of each of the other two sublattices, although the sites are far enough apart that any additional frustration is probably not an issue. This picture leads perhaps to even stronger frustration than on the simple triangular lattice, and rationalizes why the results for $n(\mu)$ and the compressibility (and perhaps other properties) are so similar in DQMC and in DMFT (which neglects intersite correlations).

### B. U-dependent Spectral Density at Half-filling

At half-filling, the MIT can also be observed through the evolution of $A(\omega)$, shown in Fig. 4. For $U$=1 eV, the spectral density has clearly begun splitting into two parts, the lower (LHB) and upper Hubbard bands (UHB). At $U$=1.5 eV, a gap has
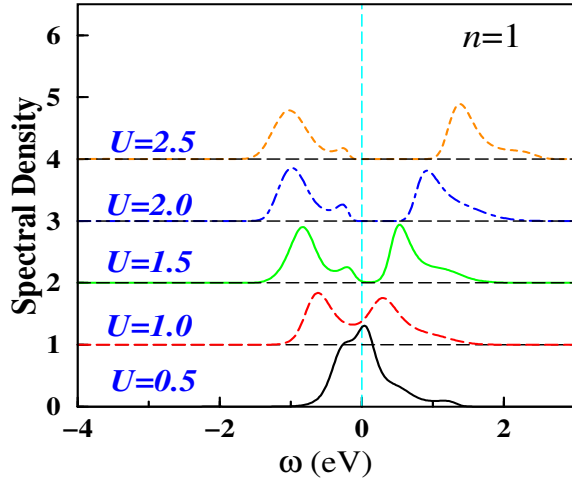
FIG. 4: (Color online) Effect of the on-site Coulomb repulsion $U$ (in units of eV) on spectral density, which is obtained from MaxEnt, for $n$=1. At $U$=1.5 eV, a gap opens clearly.

opened, consistent with the identification above of $U_c \approx 1.5$ eV. The gap increases monotonically with $U$ for stronger coupling, as expected. No peak is seen at the chemical potential as the gap opens because of the relatively high temperature used here (roughly three times higher than used by Aryanpour and collaborators[16] for the case of near neighbor hopping only).

This spectral density shows two interesting features. First, this gap opening occurs simultaneously with appearance of a low binding energy peak just below $\omega = 0$. Second, recall that within LDA ($U$=0) half of the weight lies in the lower 13% of the total bandwidth (see Fig. 1), but that at half-filling equal weight goes to the LHB and UHB. The band asymmetry fades fairly rapidly as $U$ increases, with a remnant peak on the low-binding-energy side of the LHB and the high-binding-energy tail on the UHB reflecting the structure in the underlying $U$=0 density of states (again, see Fig. 1).

In single band near-neighbor models with a single hopping $t$, the correlation strength is gauged in terms of the ratio of $U/W$ with an unambiguous bandwidth $W$. However, in the triangular lattice, the tight-binding DOS has a long high energy tail and steep lower edge, as shown in Fig. 1. This extremely asymmetric shape suggests that $W$ alone does not give a meaningful measure of the DOS. We define an effective band width $\widetilde{W}$ in terms of the second moment of the DOS. From $\widetilde{W} \approx 0.60$ eV we obtain a critical Coulomb interaction strength ratio $U_c/\widetilde{W} \approx 2.5$ for the metal-to-insulator transition.

Using DMFT(QMC), Aryanpour *et al.* investigated the half-filled triangular lattice[16] with only
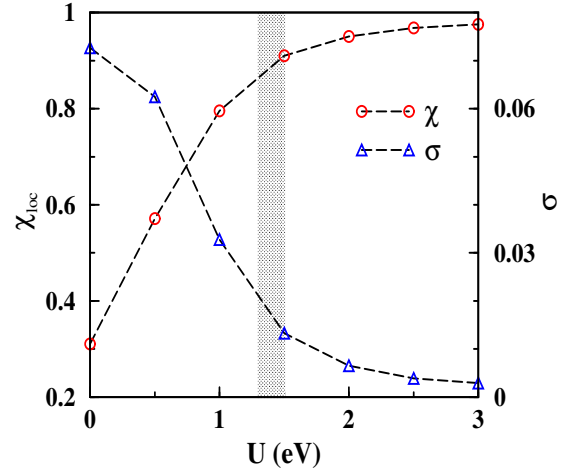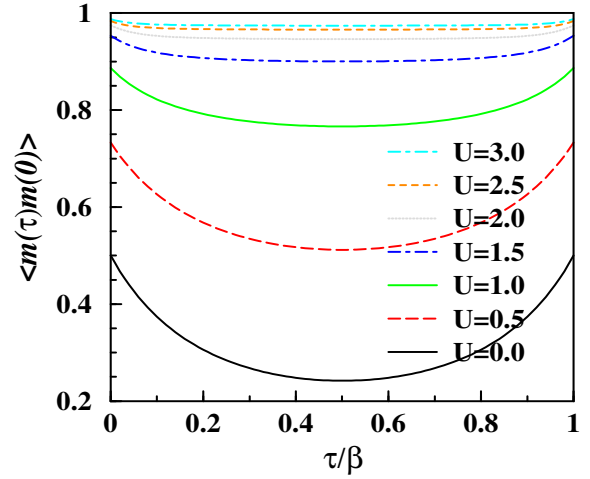




FIG. 5: (Color online) Top: Change in the correlation function $\langle m(\tau)m(0)\rangle$ of local moment $m$ as $U$ increases. Bottom: $U$-dependent local susceptibility $\chi_{loc}$ (left) and standard deviation $\sigma$ (right) over $(0,\beta)$ for the correlation function. The $\sigma$ plot shows that variance of the correlation function is strongly reduced by the transition to the insulating phase.

nearest neighbor hopping ($t = -1$ in arbitrary units) for which $\widetilde{W} \approx 4.9$ (the full bandwidth is $W = 9|t| = 9$). They obtained $U_c$=12±0.5 eV at a temperature of 400 K, or $U_c/\widetilde{W} \approx 2.5$–2.6, the same as for $Li_xNbO_2$ ($x$=0) above (carried out at 1160 K). Thus in this case the more complex dispersion and altered DOS shape has negligible effect on the critical interaction strength ratio.

### C. Local Susceptibility at Half-filling

At half-filling, the local moment $m_{rms} = \sqrt{\langle m_z^2 \rangle} \equiv \sqrt{\langle (n_\uparrow - n_\downarrow)^2 \rangle}$ increases from $\frac{1}{\sqrt{2}}$ at $U$=0

to unity for $U \to \infty$. For the half-filled system $n=1$, $m_{rms} = \sqrt{1-2d}$ where $d$ is the fraction of doubly-occupied sites. The imaginary time correlation function of the local moment $\chi(\tau) = \langle m(\tau)m(0) \rangle$ contains additional information about how the moment decorrelates in imaginary time from its value $\chi(\tau=0) = \langle m_z^2 \rangle$. As shown in Fig. 5, as $\tau$ increases in the range $[0,\beta/2]$, $\chi(\tau)$ decreases strongly when $U$ is small, whereas for $U > U_c$, $\chi(\tau)$ becomes nearly flat.

The bottom panel of Fig. 5 shows the local susceptibility $\chi_{loc} \equiv (1/\beta) \int_0^\beta \chi(\tau)d\tau$ versus $U$. When $U$ surpasses $U_c$, the local susceptibility rapidly saturates. The variance $\sigma$ of $\chi(\tau)$ from its average value ($\chi_{loc}$) is also displayed in Fig. 5. $\sigma(U)$ drops by roughly a factor of 40 between $U=0$ to $U=3$ eV, having its maximum (negative) slope around $U=1$.

## IV. NONSTOICHIOMETRIC PHASE

In this section, we will address the hole-doped phases, specifically two fillings $n=4/3$ ($Li_{\frac{1}{3}}NbO_2$, representing the regime not yet synthesized) and $n=5/3$ ($Li_{\frac{2}{3}}NbO_2$, representing the reported superconducting regime) through spectral density studies. Comparison of these results with experimental data will enable the identification of the strength of correlation effects.

### A. Correlation Effects on Spectral Density

Figure 6 shows $A(\omega)$ for $n=4/3$ and $5/3$. At $n=4/3$, even for $U=1.0$ eV, a robust lower Hubbard band (LHB) is established. By $U=1.5$ eV$=U_c$ the LHB completely separates from the more intense peak at $-0.15$ eV. The LHB is clearly identifiable and contains about 0.3 electrons per spin, which is close to the number of holes per spin $n_h=1/3$. The structure around the chemical potential and around 0.5 eV is persistent as $U$ increases, but is not monotonic and may not be above the resolution of the MaxEnt technique that is used to obtain these spectral densities. Certainly there is no obvious upper Hubbard band that shifts monotonically with $U$.

At $n=5/3$, the LHB appears for $U$ as small as 0.5 eV. Its weight is near 0.1 per spin independent of $U$, and shifts downward almost linearly with $U$; the hole-doping level is $n_h=0.17/$spin. For the main spectral weight peak around -0.5 eV and in the electron-addition spectrum, there is little change as $U$ increases. The LHB can be understood simply. In a snapshot of a doped system one would see doubly occupied sites and singly occupied sites (for substantial $U$). The process corresponding to the LHB is
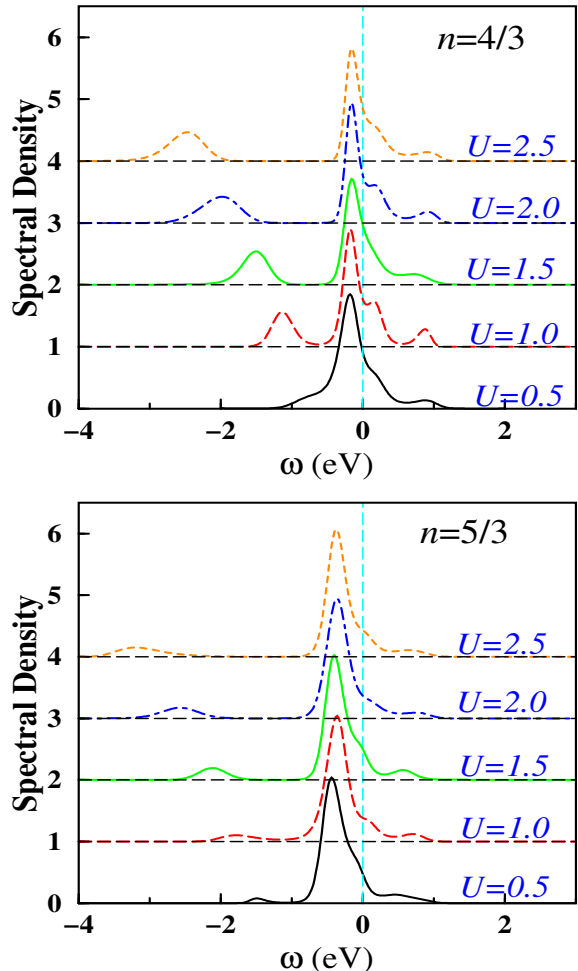


FIG. 6: (Color online) Effect of the on-site Coulomb repulsion $U$ (in units of eV) on spectral densities, which are obtained from MaxEnt, for $n=4/3$ (top) and $5/3$ (bottom). As expected from the bandwidth, correlated behavior already appears at $U=0.5$ eV. (For details, see text.) Note the spectral densities are normalized, i.e., $\int A(\omega)d\omega = 1$.

removing an electron from the singly occupied sites, so the fraction of such sites is equal to the number of holes, and thus similar to the weight of the LHB. This picture seems to be more precise for the higher hole concentration ($n=4/3$).

Cherkashenko et al. reported[20] the x-ray emission spectrum for Nb $4d \to 2p$ transitions for $Li_xNbO_2$, $x=0.97$ and 0.71, i.e. for the near band insulator and superconducting compositions respectively. With their low resolution, all that could be identified was a decrease in the occupied Nb $4d$ intensity and some narrowing, without measurable shift in the peak, as the Li concentration was reduced. This behavior is roughly consistent with a rigid band picture, if the narrowing can be as-

TABLE I: Change in direct width $W$, effective width $\widetilde{W}$ (see text for the definition), and critical $U_c$ for MIT (in units of eV) when O is displayed. The centroid of the band $E_0$ (in meV) measured from the value of $E_F$ for $n=4/3$. There is a consistent critical strength $U_c/\widetilde{W} \approx 2.5$. Each tight binding parameters (in meV) used here are from Ref. [6]. The compared DOS are shown in the top panel of Fig. 7.

| | Tight binding | | | | | | |
| | $t_1$ | $t_2$ | $t_3$ | $W$ | $\widetilde{W}$ | $E_0$ | $U_c$ |
|---|---|---|---|---|---|---|---|
| $d_+$ | 19 | 102 | 10 | 1.1 | 0.51 | -48 | 1.2 |
| $d_0$ | 64 | 100 | 33 | 1.5 | 0.60 | -18 | 1.5 |
| $d_-$ | 122 | 94 | 56 | 2.0 | 0.80 | -77 | 1.7 |



cribed to the Fermi level moving from the top of the band (insulating phase) down into the band (metallic phase). However, the edge position did not change as it would in a rigid band picture, so the interpretation is not certain. Higher resolution x-ray measurements, compared with our predictions, will be very useful in identifying correlation effects in this system.

## B. Effect of Nb–O Bond Stretching Mode

The calculations of Ylvisaker and Pickett in the band insulating phase led to a mean deformation potential $\mathcal{D} = dW/dz \sim 2.5$ eV/Å, a substantial value suggesting the importance of O displacement $\Delta z$ for electron-phonon coupling, *i.e.* transport and superconductivity.[6] To investigate effects of the O $A_g$ phonon mode on $A(\omega)$ we have used the O ion displacements $\Delta z = \pm 0.10$ Å along the $c$ direction. This displacement is representative of the maximum amplitude of the $A_g$ mode, and it happens to be similar to the variation of the S position in NbS$_2$ reported between $x=0$ and $x=0.67$ in isovalent, isostructural, and superconducting Li$_x$NbS$_2$.[24, 25] This magnitude of displacement leads to significant changes in hopping integrals, as reproduced in Table I, resulting in considerably different DOS shape for each O position.

The DOS (obtained from the tight-binding fit, but equivalent to the first principles result) displayed in the top panel of Fig. 7 shows that the most significant change is in bandwidth, about $\pm 0.5$ eV for $\mp 0.10$ Å change in O position giving the mean deformation potential mentioned above. The variation of the DOS is not well characterized simply by W however, because as W increases the portion of the DOS containing $\sim 60 - 70\%$ of the states *narrows* by roughly a factor of two. As a result, the position
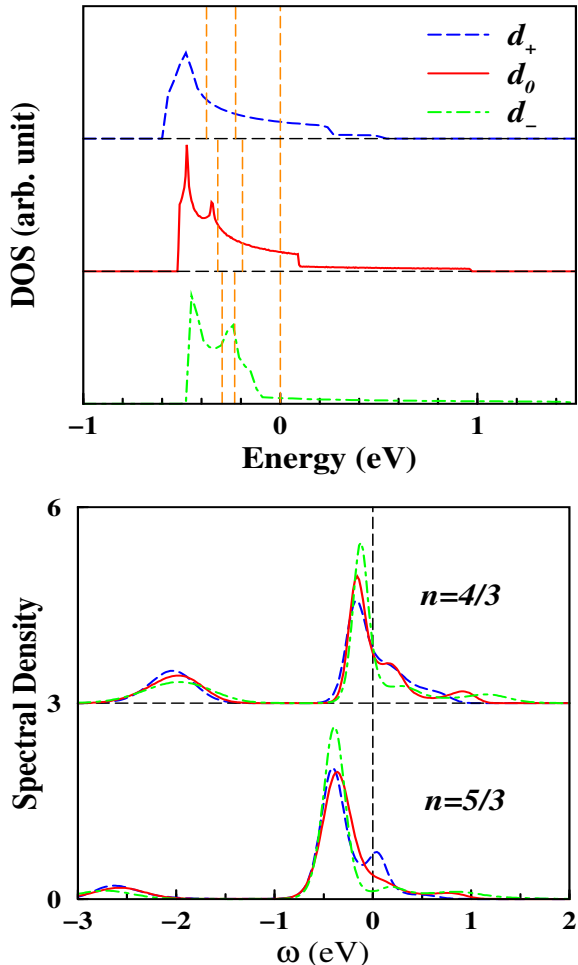
FIG. 7: (Color online) Effect of O displacement on spectral densities. O is displaced by $\pm 0.10$ Å in the $\langle 001 \rangle$ direction. $d_0$ is the optimized position. $d_-$ and $d_+$ denote contraction and elongation of the Nb–O bond length, respectively. Top: Tight-binding DOS (i.e., $U=0$) for the O displacement. The densities of states are aligned with respect to $E_F$ for $n=5/3$, set to zero. For each case, the dashed vertical lines denote $E_F$ for $n=1$, 4/3, and 5/3 (left to right). Bottom: Change in spectral densities, which shows effects of the phonon mode, at $U=2$ eV. The line designations are the same as in the top panel.

of $E_F$ and DOS at $E_F$ $N(E_F)$ change significantly for all fillings, and especially at $n = 5/3$. Since the bandwidth $W$ seems to change the most, the value $\mathcal{D} = 2.5$ eV/Å is probably an overestimate.

Considering correlation effects within our DMFT approach, O displacement affects $A(\omega)$ most strongly within $\pm 0.5$ eV of the chemical potential, as shown in the bottom panel of Fig. 7. The LHB is hardly affected, either in position or in weight. The spectral densities that are displayed are for $U=2$ eV, but for all $U$ studied here the phonon effects are sim-

ilar. At $n=5/3$, which is in the range of observed superconductivity, $A(\omega = 0)$ fluctuates strongly, while at $n=4/3$ $A(\omega = 0)$ varies little. The changes occur for $\omega$ only up to a few tenths of eV.

## V. SUMMARY

The single $d_{z^2}$ band in $Li_xNbO_2$, isolated due to large trigonal crystal field splitting, requires three neighbor hopping parameters to reproduce its dispersion, second neighbor hopping being dominant. This long range of hybridization reflects the fact that the corresponding Wannier function is not well localized, having significant O $2p$ and neighboring Nb $4d$ character in addition to the on-site $4d_{z^2}$ part. The dispersion leads to highly asymmetric DOS which contains half its weight in the lower 13% of bandwidth.

Using DMFT(QMC), we have investigated correlation effects on the spectral densities and have followed the Mott transition using both the compressibility and the spectral density. At half-filling, a metal-to-insulator transition occurs at $U_c \approx 1.5$ eV. Because of long tail and steep edge of DOS in the two-dimensional tight-banding model for the triangular lattice, however, we have introduced an effective bandwidth $\widetilde{W}$ obtained from the second moment of the density of states to characterize the band. The critical interaction strength ratio $U_c/\widetilde{W} \sim 2.5$ for the Mott transition is the same as was obtained for the triangular lattice nearest neighbor Hubbard model, indicating that the more complex dispersion does not affect the position of the metal-insulator transition in this system.

Calculation of the spin correlation functions with determinant QMC verifies that second neighbor correlations are by far the largest, as expected from the hopping parameters. Spin correlations between other neighbors are very minor. We find however that the behavior of the band filling $n(\mu)$ and the compressibility are virtually identical in DMFT (which neglects intersite spin correlations) and DQMC, justifying *a posteriori* our use of DMFT for this triangular lattice system. The dominant second neighbor hopping $t_2$ tends to partition the lattice into three weakly coupled triangular sublattices (lattice constant $\sqrt{3}$); each of these are frustrated with the antiferromagnetic coupling, and the small coupling between these sublattices adds to the frustration.

The spectral density was used to assess the strength and character of correlation effects in $Li_xNbO_2$, both for the static lattice and for frozen displacements of the O $A_g$ phonon. These results were presented for a grid of interaction ($U$) strengths, since the appropriate value for $Li_xNbO_2$ is not yet known. These results will be useful in the interpretation of high-resolution photoemission data, which are needed to further our understanding of this very interesting new triangular lattice superconductor.

[1] M. J. Geselbracht, T. J. Richardson, and A. M. Stacy, Nature **345**, 324 (1990).

[2] P. Bordet, E. Moshopoulou, S. Liesert, and J. J. Capponi, Physica C **235-240**, 745 (1994).

[3] E. G. Moshopoulou, P. Bordet, and J. J. Capponi, Phys. Rev. B **59**, 9590 (1999).

[4] G. T. Liu, J. L. Luo, Z. Li, Y. Q. Guo, N. L. Wang, D. Jin, and T. Xiang, Phys. Rev. B **74**, 012504 (2006).

[5] D. G. Kellerman, G. P. Shveikin, A. P. Tyutyunnik, V. G. Zubkov, V. A. Perelyaev, T. V. D'yachkova, N. I. Kadyrova, A. S. Fedyukov, S. A. Turzhevskii, V. A. Gubanov, G. P. Shveikin, A. E. Karkin, and V. I. Voronin, Superconductivity:Phys. Chem. Tech. **5**, 2035 (1992).

[6] E. R. Ylvisaker and W. E. Pickett, Phys. Rev. B **74**, 075104 (2006).

[7] E. R. Ylvisaker, K.-W. Lee, and W. E. Pickett, Physica B **383**, 63 (2006).

[8] D. L. Novikov, V. A. Gubanov, V. G. Zubkov, and A. J. Freeman, Phys. Rev. B **49**, 15830 (1994).

[9] D. G. Kellerman, V. G. Zubkov, A. P. Tyutyunnik, V. S. Gorshkov, V. A. Perelyaev, G. P. Shveikin, S. A. Turzhevskii, V. A. Gubanov, and A. E. Karkin, Superconductivity:Phys. Chem. Tech. **5**, 966 (1992).

[10] A. P. Tyutyunnik, V. G. Zubkov, D. G. Kellerman, V. A. Perelyaev, A. E. Karkin, and G. Svensson, Eur. J. Solid State Inorg. Chem. **33**, 53 (1996).

[11] N. Kumada, S. Watauchi, I. Tanaka, and N. Kinomura, Mater. Res. Bull. **35**, 1743 (2000).

[12] E. Morosan, H. W. Zandbergen, B. S. Dennis, J. W. G. Bos, Y. Onose, T. Klimczuk, A. P. Ramirez, N.

P. Ong, and R. J. Cava, Nature Phys. **2**, 544 (2006).

[13] K.-W. Lee, J. Kuneš, and W. E. Pickett, Phys. Rev. B **70**, 045104 (2004); K.-W. Lee, J. Kuneš, P. Novak, and W. E. Pickett, Phys. Rev. Lett. **94**, 026403 (2005); K.-W. Lee and W. E. Pickett, *ibid.* **96**, 096403 (2006).

[14] V. Eyert, Europhys. Lett. **58**, 851 (2002); references therein.

[15] For review, see A. Georges, G. Kotliar, W. Krauth, and M. J. Rozenberg, Rev. Mod. Phys. **68**, 13 (1996); G. Kotliar, S. Y. Savrasov, K. Haule, V. S. Oudovenko, P. Parcollect, and C. A. Marianetti, *ibid.* **78**, 865 (2006).

[16] K. Aryanpour, W. E. Pickett, and R. T. Scalettar, Phys. Rev. B **74**, 085117 (2006).

[17] N. Kumada, S. Muramatu, F. Muto, N. Kinomura, S. Kikkawa, and M. Koizumi, J. Solid State Chem. **73**, 33 (1988).

[18] G. Meyer and R. Hoppe, Angew. Chem., Int. Ed. Engl. **13** (1974); J. Less-Common Met. **46**, 55 (1976).

[19] M. J. Geselbracht, A. M. Stacy, A. R. Garcia, B. G. Silbernagel, and G. H. Kwei, J. Phys. Chem. **97**, 7102 (1993).

[20] V. M. Cherkashenko, M. A. Korotin, V. I. Anisimov, V. V. Shumilov, V. R. Galakhov, D. G. Kellerman, V. G. Zubkov, and E. Z. Kurmaev, Z. Phys. B **93**, 417 (1994).

[21] K. Koepernik and H. Eschrig, Phys. Rev. B **59**, 1743 (1999).

[22] M. Jarrell and J. E. Gubernatis, Phys. Rep. **269**, 133 (1996).

[23] R. Blankenbecler, D. J. Scalapino, and R. L. Sugar Phys. Rev. D **24**, 2278 (1981).

[24] P. A. Salyer, M. G. Barker, A. J. Blake, D. H. Gregory, and C. Wilson, Acta Crystallogr. C**59**, i4 (2003).

[25] F. Jellinek, G. Brauer, and H. Müller, Nature (London) **185**, 376 (1960).